
Volume 16, Issue 4, 162529 (1-15)

International Journal of Nano Dimension (IJND)

https://dx.doi.org/10.57647/j.ijnd.2025.1604.29

# Synthesis, characterization of Graphene Oxide/ZnO/$Al_2O_3$ nanocomposite Aerogel and its electrochemical application

Barakat Abdul-Fattah Kamil*, Dhia Hadi Hussain

*Department of Chemistry, College of Science, Al-Mustansiriyah University, Baghdad, Iraq.*

***Corresponding author:** baraka1983@uomustansiriyah.edu.iq

**Original Research**

Received:
12 January 2025
Revised:
10 April 2025
Accepted:
1 May 2025
Published online:
10 May 2025
Published in issue:
17 May 2025



**Abstract:**

In this study, nanocomposite GO/ZnO/$Al_2O_3$ aerogels with different GO ratios (10, 30, and 50%) were effectively prepared using a hydrothermal method and a modified Hummers method to prepare GOES. ZnO and $Al_2O_3$ NPs were synthesized from curcumin extract using a green synthesis method. Raman, XRD, EDX, FESEM and UV-Vis. Spectra were used to characterize the synthesized nanomaterials. The bandgap energies of GO, ZnO, $Al_2O_3$, and their nanocomposites were calculated from their UV spectra. The interaction between the components of the nanocomposite graphene oxide, zinc oxide and aluminum oxide give the nanocomposite photochemical importance owing to the large surface area of the components, especially graphene oxide and zinc oxide, and the high electrical and thermal conductivities of the molecule. Improved electrochemical properties were achieved by fabricating dye-sensitized solar cells, composed of nano curcumin and methylene blue as sensitizers, GO/ZnO/$Al_2O_3$ nanocomposite aerogel as a photoanode to obtain a highly efficient cell at the lowest cost and copper as the counter electrode. The DSSC achieves the best performance at 0.36% and 50% GO content when methylene blue is used as a sensitizer to accelerate the excitation of electrons and generate current and voltage. The primary objective of this study is to develop dye-sensitized solar cells with maximum efficiency at minimum cost.

**Keywords:** Electrochemical Application and Dye-Sensitized Solar Cell (DSSC); FESEM; Graphene oxide; Nanocomposite Aerogel; Nanocurcumin

## 1. Introduction

The aerogel was created by substituting gas for liquid in the wet gel without appreciably altering the volume or structure of the gel network. Aerogel has high specific surface area and porosity and low density. When combined with other matrix components, such as graphene and its byproducts, graphene oxide (GO) and reduced GO (rGO), a graphene-based composite aerogel (GCA) is formed. The primary source of the functions of graphene and its derivatives, or graphene-based materials, differs from that of conventional matrix materials, which mainly define their shape and volume stability [1]. GCA is not only a damping, adsorbing, thermal, and sound-absorbing material but can also be used as an electrode material in sensors and energy storage devices [2]. Solar energy is the most abundant, renewable, accessible, unlimited source of energy, and can be converted into usable energy [3]. Graphene aerogels and their composites used in dye-sensitized solar cells (DSSCs), which have attracted great interest since Gratzel and O'Regan's breakthrough in 1991 as an alternative to fossil fuels are inexpensive, require little energy, easy to manufacture and environmentally friendly [4]. The photoanode in a typical DSSC is a dye-sensitized semiconducting metal oxide, in combination with an electrolyte redox and counter electrode [5]. Various organic and inorganic semiconductors are mainly used in hybrid photovoltaics (PV) as solar energy harvesters because of their excellent power conversion efficiency (PCE), low cost, and ease of manufacturing [6]. For example, $TiO_2$, $Al_2O_3$ and ZnO are used as photoanode materials in DSSC, owing to their supercharge carrier transport properties and due to their significant bandgaps, these semiconductors exhibit low PCE, significant carrier recombination, and poor carrier transport [7, 8]. To address these problems, carbon-dependent substances, such as GO have been introduced as alternatives or complements to $Al_2O_3$ and ZnO to facilitate electron transfer to the con-

nected transparent pole [9]. GO sheets can be highly oxidized and contain important functional combinations, such as alcohols, carboxylic acids, and epoxides. The oxygen-containing functional groups on GO render the material hydrophilic and easily dispersible in water. Further, GO can accommodate most nanoparticles because of its exceptional electrical conductivity, large specific surface area, and high chemical stability [10] Therefore, this study prepared, a GO/ZnO/$Al_2O_3$ nanocomposite aerogel and used it as a photoanode electrode. The photochemical characteristics of each constituent, particularly zinc oxide and graphene oxide, endow the nanocomposite with a wide surface area, increasing the number of active sites available for photochemical reactions. Dye sensitizers have a significant impact on light absorption and thus on the efficiency of DSSCs. When light activates the chemical structure of a sensitizing dye; that share could be it generates electron-hole pairs, which determine the performance of a conventional DSSC. The dye in DSSCs converts light into electronic excitation by transferring charge to the semiconductor surface figure 1 shows the DSSC mechanism [11]. Nano curcumin is a natural dye and methylene blue is a synthetic dye, which was used as a sensitizer. It has sufficient potential for application in photochemical processes. These easily accessible dyes create appropriate catalytic pathways including both single-electron transfer (SET) and energy transfer (EnT); while utilizing visible light as a renewable energy source.

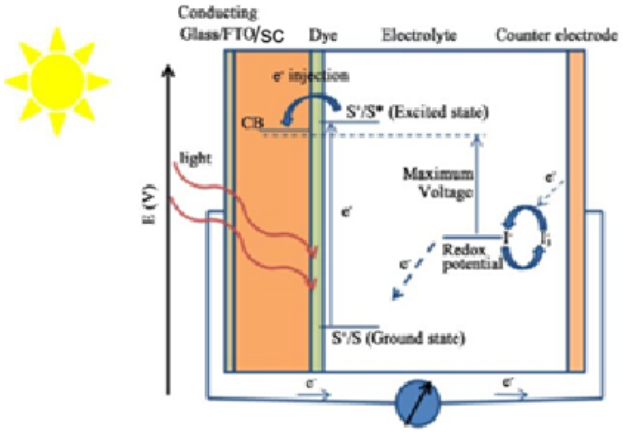


**Figure 1.** The Diagram of DSSC Mechanism.

## 2. Materials and methods

Zinc acetate hexahydrate ($Zn(CH_3COO)_2{\cdot}6H_2O$) (99%), aluminum nitrate nonahydrate ($Al(NO_3)_3{\cdot}9H_2O$) (99%), sodium hydroxide (NaOH) (98%), sulfuric acid ($H_2SO_4$) (97%), phosphoric acid ($H_3PO_4$) (85%), graphite (99%), potassium permanganate ($KMnO_4$) (99%), hydrogen peroxide ($H_2O_2$) (99%), hydrochloric acid (HCl) (99%), ethylene diamine ($C_2H_8N_2$) (98%), methylene blue (99%) were all supplied by Sigma-Aldrich. Fresh turmeric (Curcuma longa) was also used.

### 2.1 Preparation of curcumin extract

Fresh turmeric was thoroughly washed and dried, and then ground into fine powder using a grinder. Deionized water (100 mL) was added to 10 g of turmeric powder and boiled at 60 °C with stirring for 1 h. The turmeric extract was cooled to room temperature and filtered to obtain a clear curcumin extract [12].

### 2.2 Preparation of zinc oxide and aluminum oxide nanoparticles from curcumin extract

The curcumin extract (10 mL) was added to 100 mL of 0.5 M $Zn(CH_3COO)_2{\cdot}6H_2O$ or $Al(NO_3)_3{\cdot}9H_2O$ solutions and kept on a magnetic stirrer. To maintain the pH at 8, 2 M of NaOH was added dropwise. The mixture was stirred and heated at 70 °C for two hours to achieve complete reduction and the development of a white precipitate. Subsequently, the resulting material was collected by decantation, washed with deionized water to remove residues, and dried in an oven at 70 °C. The resulting powders were calcined at 400 °C for zinc oxide and 500 °C for aluminum oxide to obtain ZnO and $Al_2O_3$ nanoparticle powders, respectively [13].

### 2.3 Preparation of graphene oxide

GO was synthesized from graphite using the modified Hummers method. Briefly, 1 g of graphite was added to (30 mL of concentrated sulfuric acid ($H_2SO_4$) and 3.3 mL of concentrated phosphoric acid ($H_3PO_4$)) with constant stirring for 30 min. To avoid overheating and explosion, 6 g of potassium permanganate ($KMnO_4$) was gradually added, while maintaining the temperature below 20 °C. The above solution was heated at 35 °C for 2 h. Subsequently, 10 mL of 30% hydrogen peroxide ($H_2O_2$) and 100 mL of $H_2O$ were added to stop the reaction with $KMnO_4$ and the mixture was left overnight. The final mixture was centrifuged, filtered, and dried to obtain GO sheets. The samples further were cleaned using HCl or $H_2O$ [14].

### 2.4 Preparation of graphene oxide/ZnO/$Al_2O_3$ nanocomposite Aerogel

GO/ZnO/$Al_2O_3$ nanocomposite aerogel was prepared in different ratios of GO (10, 30, 50)% [15] according to the following scheme in figure 2.

### 2.5 Preparation of nanocurcumin

5 g of curcumin was dissolved in an ethanoic solution (ethanol and deionized water in a ratio of [1:9]) and ultrasonically agitated at 300 Hz for 3 h [16].

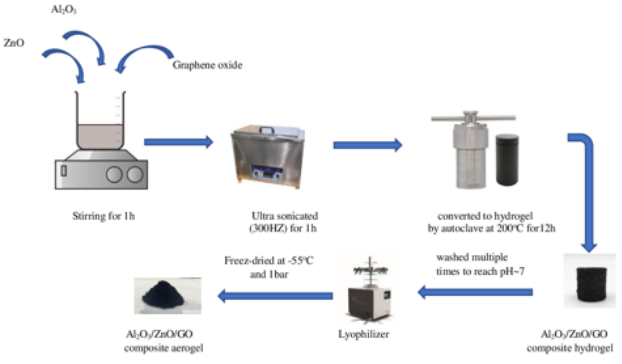


**Figure 2.** Scheme for the preparation of GO/ZnO/$Al_2O_3$ nanocomposite aerogel.

### 2.6 Fabrication of dye-sensitized solar cell

To prepare the GO/ZnO/$Al_2O_3$ nanocomposite aerogel paste, 1 g of the nanocomposite, 10 mL of ethanol, and 2 drops of Triton X-100 were mixed and magnetically stirred until the mixture reached a colloidal state. The nanocomposite paste was applied to a conductive glass substrate using spin coating at 1300 rpm for 30 seconds by achieving thickness of 8 µm [17]. The working electrode of the nanocomposite layer was then dipped into the dyes (nanocurcumin or methylene blue) and dried at 150 °C for 30 min. the counter electrode was a copper wire 15 cm in length, which was bent to form a circular shape; then placed on the FTO. To prepare the electrolyte solution, $I_2$ (3 g) was dissolved in 50 mL of ethylene glycol and 1.5 g of KI, which was stirred for 1.5 hours and kept in a dark container. Then, two drops of the electrolytic solution were added between the working and counter electrodes. For the I-V characterization analysis, the solar cell was immediately measured using a potentiostat (Model: Ossila). Solar cell performance data were obtained from previous studies [18, 19]. Figure 3 shows an image of the dye-sensitized solar cell and figure 4 shows the system of DSSC measurements.

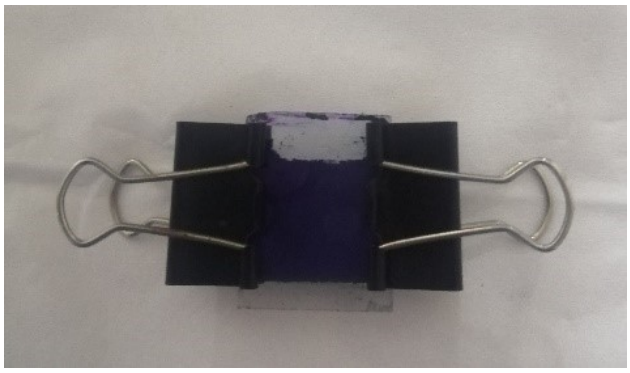

**Figure 3.** Dye-sensitized solar cell image.

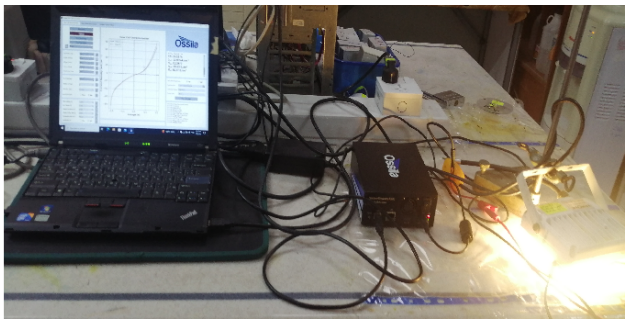

**Figure 4.** Dye-sensitized solar cell system.

## 3. Results and discussion

### 3.1 Raman spectra analysis

Figures 5 (a-c) show the Raman spectra of the synthesized GO, ZnO, and $Al_2O_3$ NPs as well as the assembled GO/ZnO/$Al_2O_3$ aerogel. These spectra enabled the study of conjugated and carbon-carbon double bonds, which result in high-intensity peaks in the Raman spectrum. The typical Raman spectrum of GO is characterized by a G band at 1648 $cm^{-1}$ attributed to the defects in the structure and a *D* band at 1447 $cm^{-1}$ reflecting carbon vibrations in the packed form. The Raman spectrum values for ZnO and $Al_2O_3$ were closed; The prominent peaks were (620 and 893) $cm^{-1}$ and (614 and 896) $cm^{-1}$ [20], while the composite was observed in different ratios for 10% GO at (617, 904, 1435 and 1654) $cm^{-1}$, for 30% GO at (626, 894, 1431 and 1637) $cm^{-1}$ and for 50% GO at (613, 903, 1443, and 1659) $cm^{-1}$, which are slightly shifted from the position of GO, ZnO, and $Al_2O_3$. The specific peaks in the Raman spectra confirm the successful integration of ZnO, $Al_2O_3$, and GO into the nanocomposite. These materials hold potential for use in fuel cells, batteries, and electronic devices due to enhanced conductivity, increased surface activity, and accelerate reactions, all of which affect the electrochemical performance.

### 3.2 Powder X-Ray diffraction (XRD) analysis

Figure 6 shows the XRD patterns of the prepared compounds. The strong, intense peak at $2\theta = 10.52°$ with 42.35° corresponds to the (001) and (100) planes of GO; and crystal sizes of 8.5 with 4.3 nm, which were calculated using the Scherrer equation. The peaks at $2\theta = 34.3°$ with 36.12° are consistent with the (002) and (101) planes of ZnO; and crystal sizes of 20, 3, 31.4, and 30.5 nm [21]. The peaks at $2\theta = 37.06°$ and 37.71° correspond to the plane (104) plane of $Al_2O_3$ and the crystal sizes (1.9 and 3) nm. For the GO/ZnO/$Al_2O_3$ nanocomposite aerogel, the ratio (10%) shows peaks at $2\theta = (11.48° - 98.5°)$ with crystal sizes $(2.9 - 67.5)$ nm, the ratio (30%) has peaks at $2\theta = (11.45° - 95.57°)$ with crystal sizes $(0.8 - 26.7)$ nm and the ratio (50%) has peaks at $2\theta = (11.28° - 54.66°)$ with crystal sizes $(1.4 - 69.4)$ nm. As shown in the figure, new peaks appear, indicating the formation of the composite. Nanocurcumin was synthesized as a sensitizer for DSSCs. Therefore, figure 7 shows the XRD pattern of nano-curcumin, whose peak value is at $2\theta = 20.067°$. With increasing the amount of graphene oxide, the intensity of the zinc oxide band becomes weak by the interaction with graphene oxide. This interaction alters the crystal size and mechanical properties, thus affecting the particle size and internal stress.

$$D = \frac{K\lambda}{\beta \cos\theta} \tag{1}$$

where $\theta$ is the Bragg angle, $\beta$ is the peak's full width at half maximum (FWHM), $\lambda$ is the wave length of the employed X-ray beam (1.54184 Å), and $K$ is the Scherrer constant.

### 3.3 EDX analysis

EDX was used to examine the percentages of atoms in the prepared compounds. Figure 8 presents the EDX of the ZnO NPs, with Zn and O contents of 66.1% and 21.3%, respectively, indicating the purity and low impurity content in ZnO NPs [22]. The EDX of $Al_2O_3$ in the figure 9; shows Al and O contents of 40.5% and 53.6%, respectively. The EDX spectrum of GO in figure 10 shows C and O contents of respectively 46.6% and 51.3%, and an amount of sulfur from sulfuric acid used in the synthesis. The EDX spectra of the GO/ZnO/$Al_2O_3$ composite aerogels show different

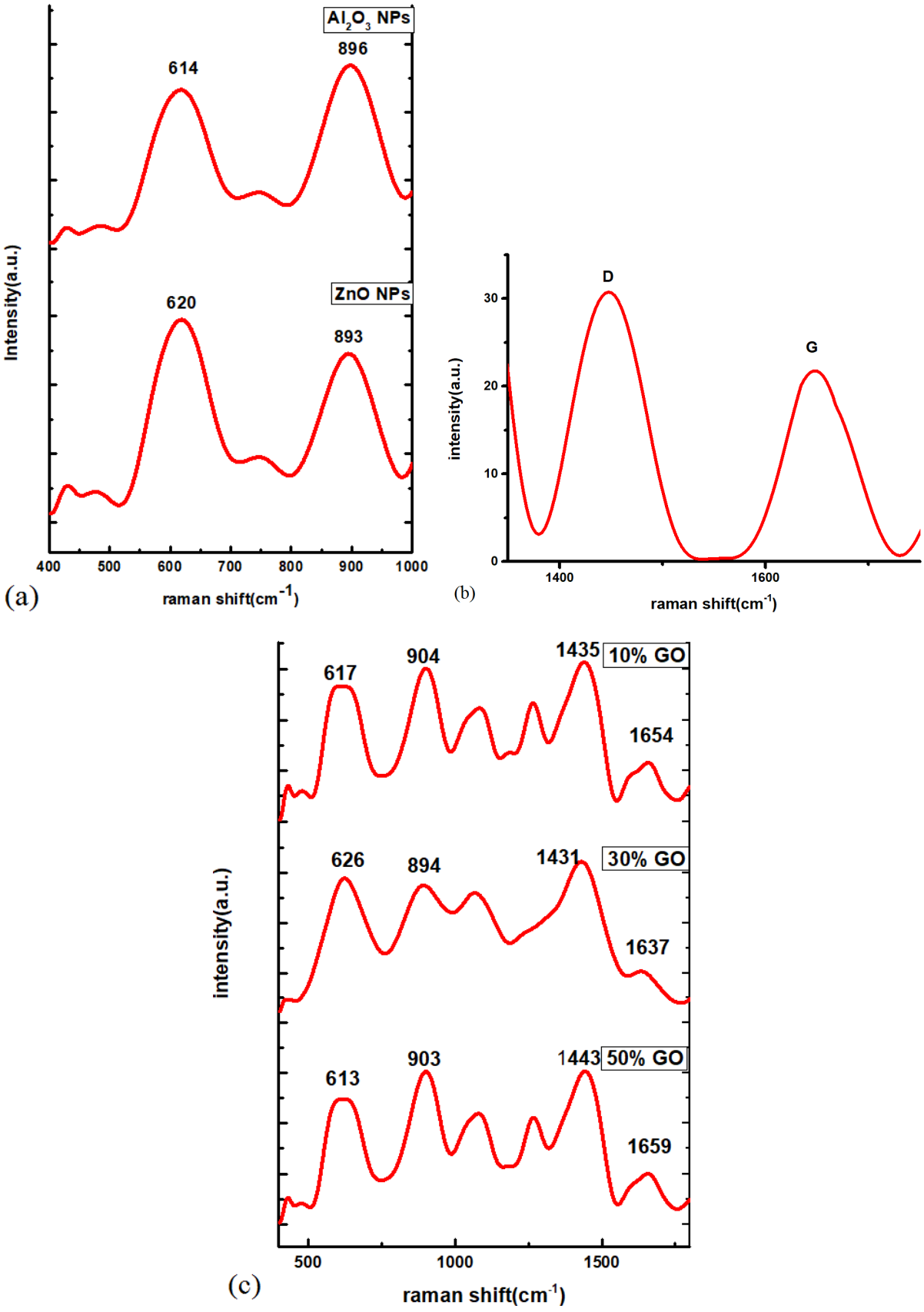


**Figure 5.** Raman Spectra of (a) GO (b) ZnO and $Al_2O_3$ NPs (c) GO/ZnO/$Al_2O_3$ nanocomposite aerogel.

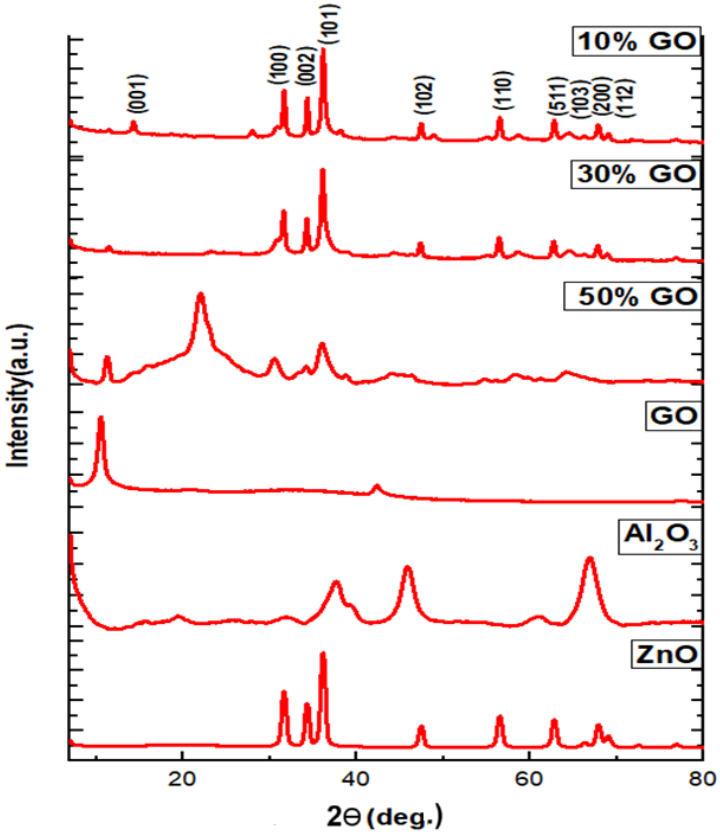


**Figure 6.** XRD Pattern of ZnO, $Al_2O_3$ and composite Aerogel (10, 30, 50)%.

percentages of C and O for the different GO contents (10, 30 and 50%) in the composite as shown in figures 11, 12, and 13. Figure 14 shows the EDX spectra of nano-curcumin with C and O contents of respectively 38.7% and 51.7%, with a few percentages of elements.

### 3.4 FESEM analysis

The morphological analysis of the synthesized nanoparticle samples was performed using FESEM; figure 15 (a), for ZnO NPs shows a flower-shaped structure with a particle diameter in the range 40.42 – 53.75 nm for one petal in ZnO NPs. The FESEM image of $Al_2O_3$ NPs in figure 15 (b), shows the formation of spherical and rod-shaped particles 34.77 – 49.53 nm in diameter. The FESEM images of GO in figure 15 (c) show distinct graphene oxide flakes with comparatively large surface areas and clearly defined connected three-dimensional layers [23]. The particle diameter is 21.99 – 33.03 nm. Figures 15 (d), 15 (e), and 15 (f) show the FESEM images of the GO/ZnO/$Al_2O_3$ nanocomposite aerogels at different GO ratios (10, 30, and 50%). The higher the GO content in the composite has provided the smaller the particle diameter. The FESEM image of nano-

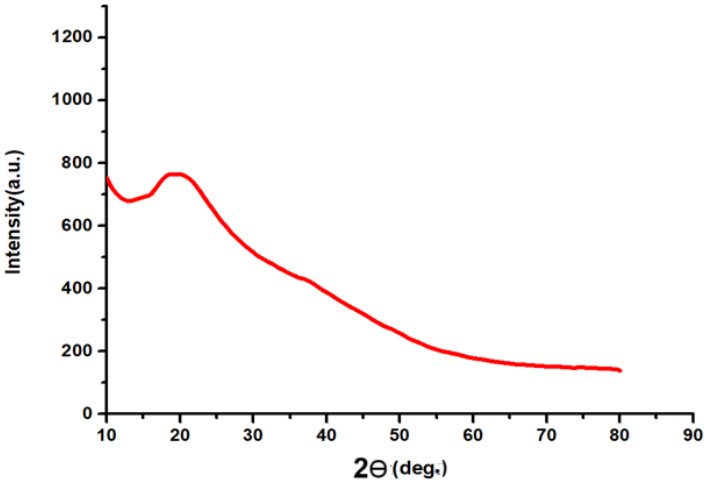


**Figure 7.** XRD pattern of nanocurcumin.

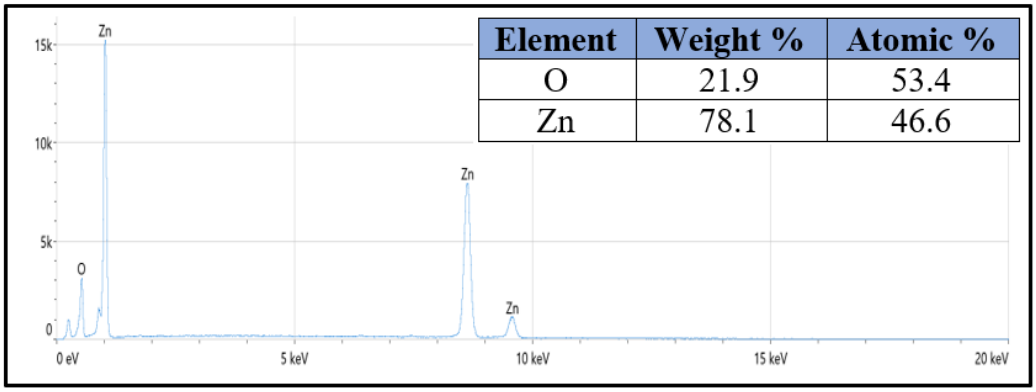


| Element | Weight % | Atomic % |
|---|---|---|
| O | 21.9 | 53.4 |
| Zn | 78.1 | 46.6 |

**Figure 8.** EDX analysis of ZnO NPs.

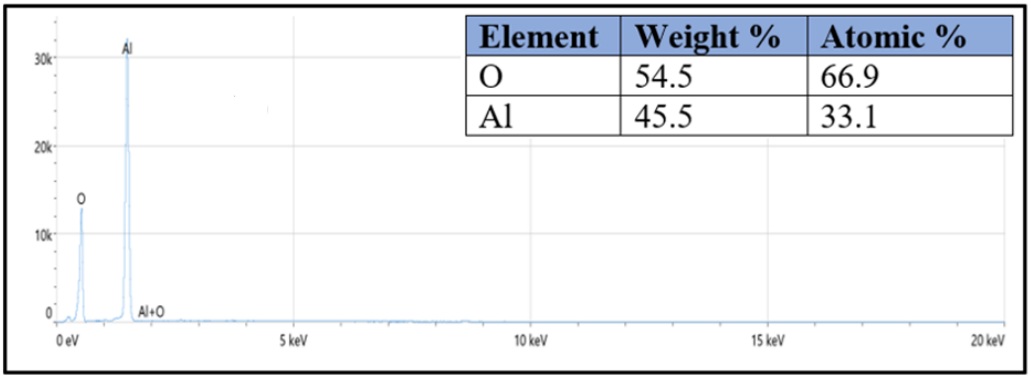


| Element | Weight % | Atomic % |
|---|---|---|
| O | 54.5 | 66.9 |
| Al | 45.5 | 33.1 |

**Figure 9.** EDX analysis of $\gamma$-$Al_2O_3$ NPs.

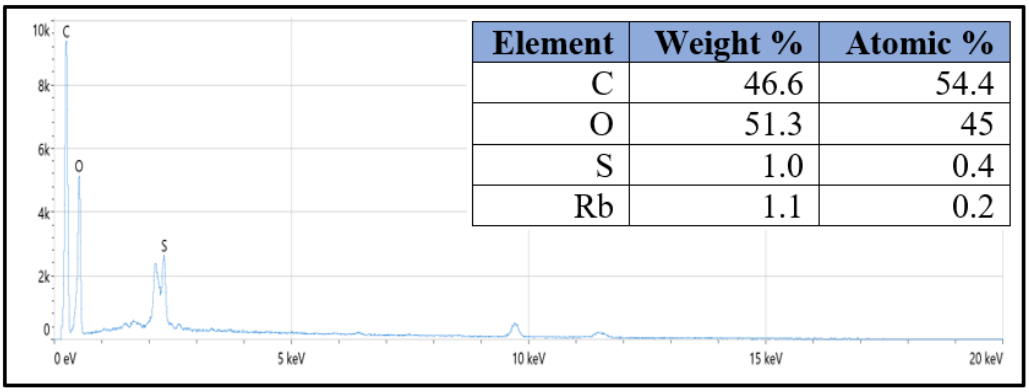


| Element | Weight % | Atomic % |
|---|---|---|
| C | 46.6 | 54.4 |
| O | 51.3 | 45 |
| S | 1.0 | 0.4 |
| Rb | 1.1 | 0.2 |

**Figure 10.** EDX analysis of GO NPs.

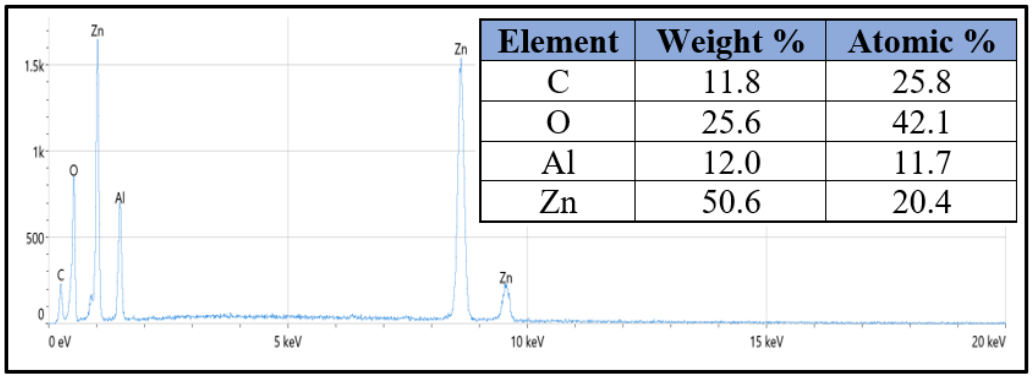


| Element | Weight % | Atomic % |
|---|---|---|
| C | 11.8 | 25.8 |
| O | 25.6 | 42.1 |
| Al | 12.0 | 11.7 |
| Zn | 50.6 | 20.4 |

**Figure 11.** EDX analysis of GO/ZnO/$Al_2O_3$ nanocomposite aerogel with GO of 10%.

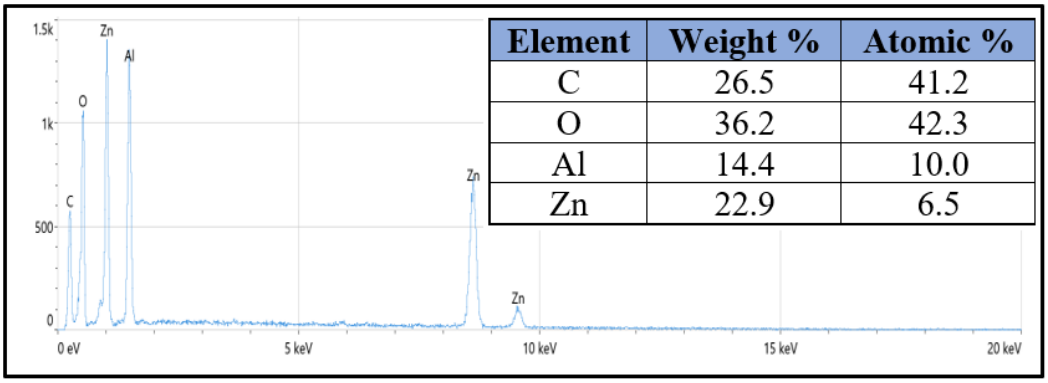


| Element | Weight % | Atomic % |
|---|---|---|
| C | 26.5 | 41.2 |
| O | 36.2 | 42.3 |
| Al | 14.4 | 10.0 |
| Zn | 22.9 | 6.5 |

**Figure 12.** EDX analysis of GO/ZnO/$Al_2O_3$ nanocomposite aerogel with GO of 30%.

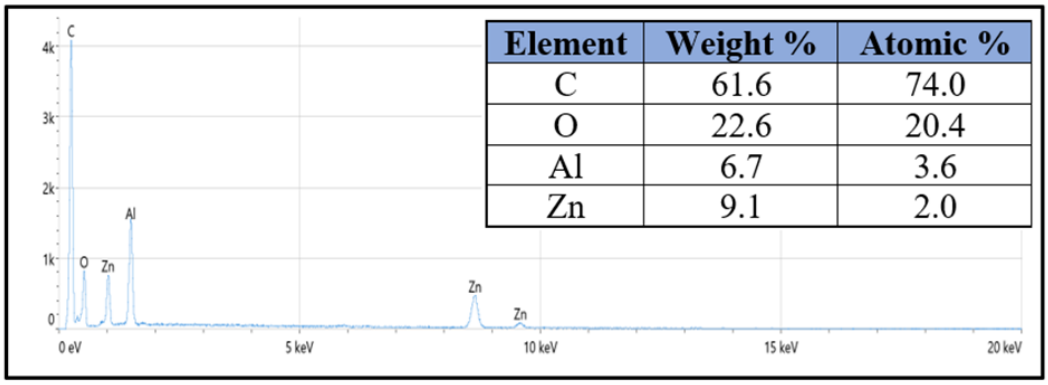


| Element | Weight % | Atomic % |
|---|---|---|
| C | 61.6 | 74.0 |
| O | 22.6 | 20.4 |
| Al | 6.7 | 3.6 |
| Zn | 9.1 | 2.0 |

**Figure 13.** EDX analysis of GO/ZnO/$Al_2O_3$ nanocomposite aerogel with GO of 50%.

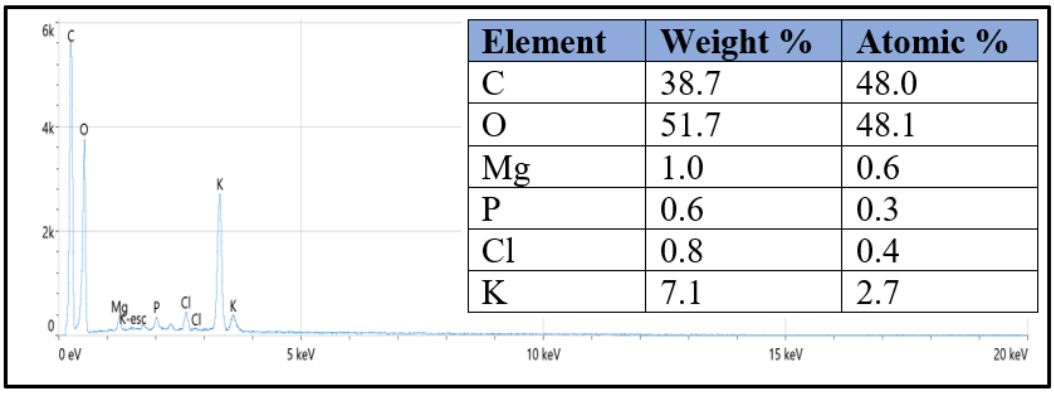


| Element | Weight % | Atomic % |
|---|---|---|
| C | 38.7 | 48.0 |
| O | 51.7 | 48.1 |
| Mg | 1.0 | 0.6 |
| P | 0.6 | 0.3 |
| Cl | 0.8 | 0.4 |
| K | 7.1 | 2.7 |

**Figure 14.** EDX analysis of Nanocurcumin.

curcumin in figure 15 (g) shows particles $36.75 - 52.42$ nm in diameter. The particles constituting the composite change their shape as the amount of GO increases, appearing smoother or more uniform in shape. The ZnO and $Al_2O_3$ particle sizes are expected to decrease with increasing GO content, which could increase the aggregation density or particle agglomeration. By increasing the GO content, surface characteristics such as porosity and roughness can be improved, which influences how the material interacts with its surroundings.

### 3.5 Optical properties

Two different electronic transitions are seen in GO, the $\pi - \pi*$ transition and the $n - \pi*$ transition. Usually, light in the visible or ultraviolet spectrum is absorbed as a result of the $\pi - \pi*$ transition, which occurs at 239 nm. This change is associated with the delocalized $\pi$ bonding network in the graphene plane. However, the oxygen-containing functional groups on the graphene surface are linked to the $n - \pi*$ electronic transition, which occurs at 313 nm. The functional groups in GO can modify the electronic structure of the graphene lattice, such as by opening a bandgap, which can drastically modify the optical and electrical characteristics of the material. Figure 16 (a) shows the UV spectra and band gap energy of GO. Figure 16 (b) shows the absorption peak of ZnO appears at 382 nm in the UV region, which is a characteristic of wurtzite hexagonal- phase ZnO. The band gap is the separation between the lowest empty conduction

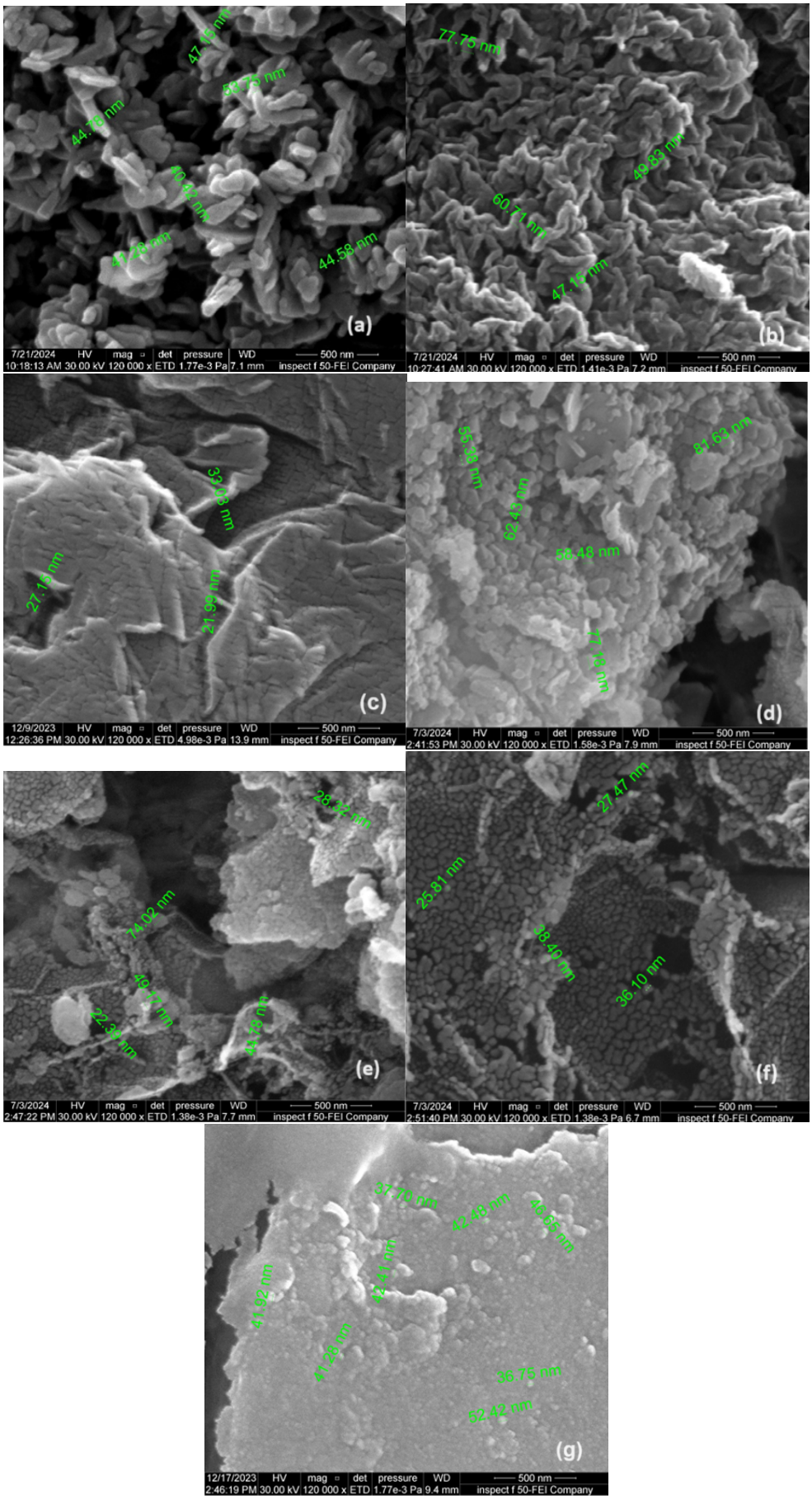


**Figure 15.** FESEM Images of, (a) ZnO, (b) $Al_2O_3$, (c) GO, (d) composite Aerogel of 10%, (e) 30%, (f) 50%, (g) Nanocurcumin.

band and the valence band of a semiconductor. It establishes the amount of photon energy that must be absorbed by the semiconductor for photoelectron and hole photogeneration to occur, figure 16 (c) depicts the UV-Vis spectra and band gap of $Al_2O_3$ NPs, revealing a peak at 262 nm, which is attributed to the photoexcitation of electrons from the valence to the conduction band. The optical properties of the GO/ZnO/$Al_2O_3$ aerogel nanocomposite with different GO ratios (10, 30% and 50%) were elucidated using UV-Vis. spectroscopy. Figures 16 (d), 16 (e), and 16 (f), show, that the peak intensities decrease with increasing ZnO concentration. By projecting the linear part of the curves onto the intersection with the $h\nu$ axis based on this relationship, the optical band gap energies were calculated using the Tauc plot of the UV-Vis data in Table 1.

$$(\alpha h\nu)^{1/n} = A(h\nu - E_g) \quad (2)$$

$h\nu$ is the photon energy, $A$ is a constant, and $\alpha$ is the absorption coefficient when $n = 2$ indicates indirect permitted transitions [24].

From Table 1, we concluded that an increase in GO amount is seen to increase the band gap energy of all the composites due to the blue shift in the wavelength, which can be attributed to the reduction of ZnO and $Al_2O_3$ sizes.

### 3.6 Photochemical properties

The photochemical properties of the prepared compounds were studied by measuring the efficiency of dye-sensitized solar cells fabricated using GO/ZnO/$Al_2O_3$ nanocomposite aerogels at different GO ratios (10, 30 and 50%) as the photoanode. Figures 17 (a), 17 (b), 17 (c), Figures 18 (a), 18 (b), 18 (c), and Figures 19 (a), 19 (b), 19 (c) show the I-V curves of the fabricated dye-sensitized solar cells.

Table 2 shows the efficiencies of dye-sensitized solar cells in different ratios of nanocomposite aerogel (10, 30, and 50)

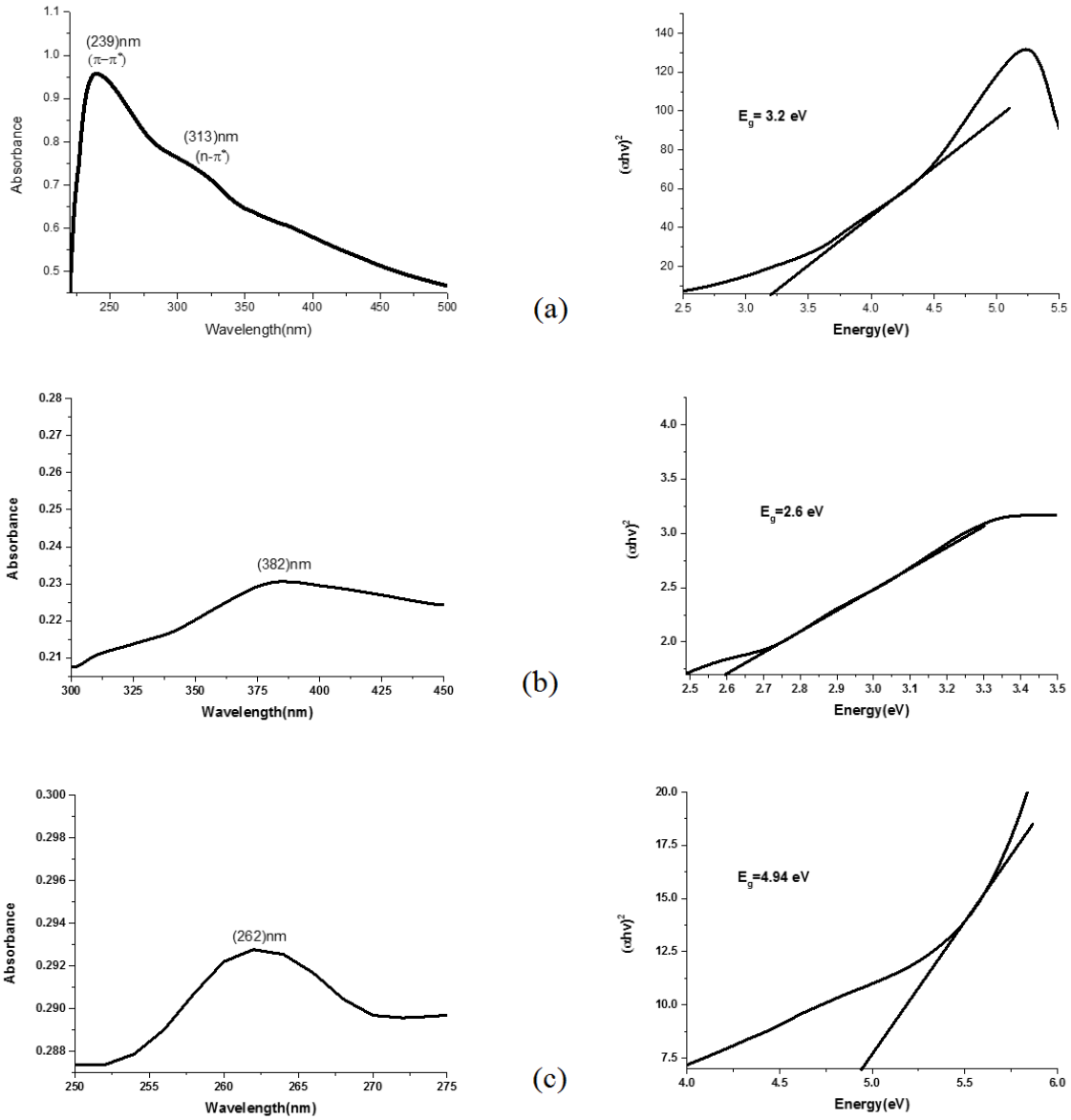

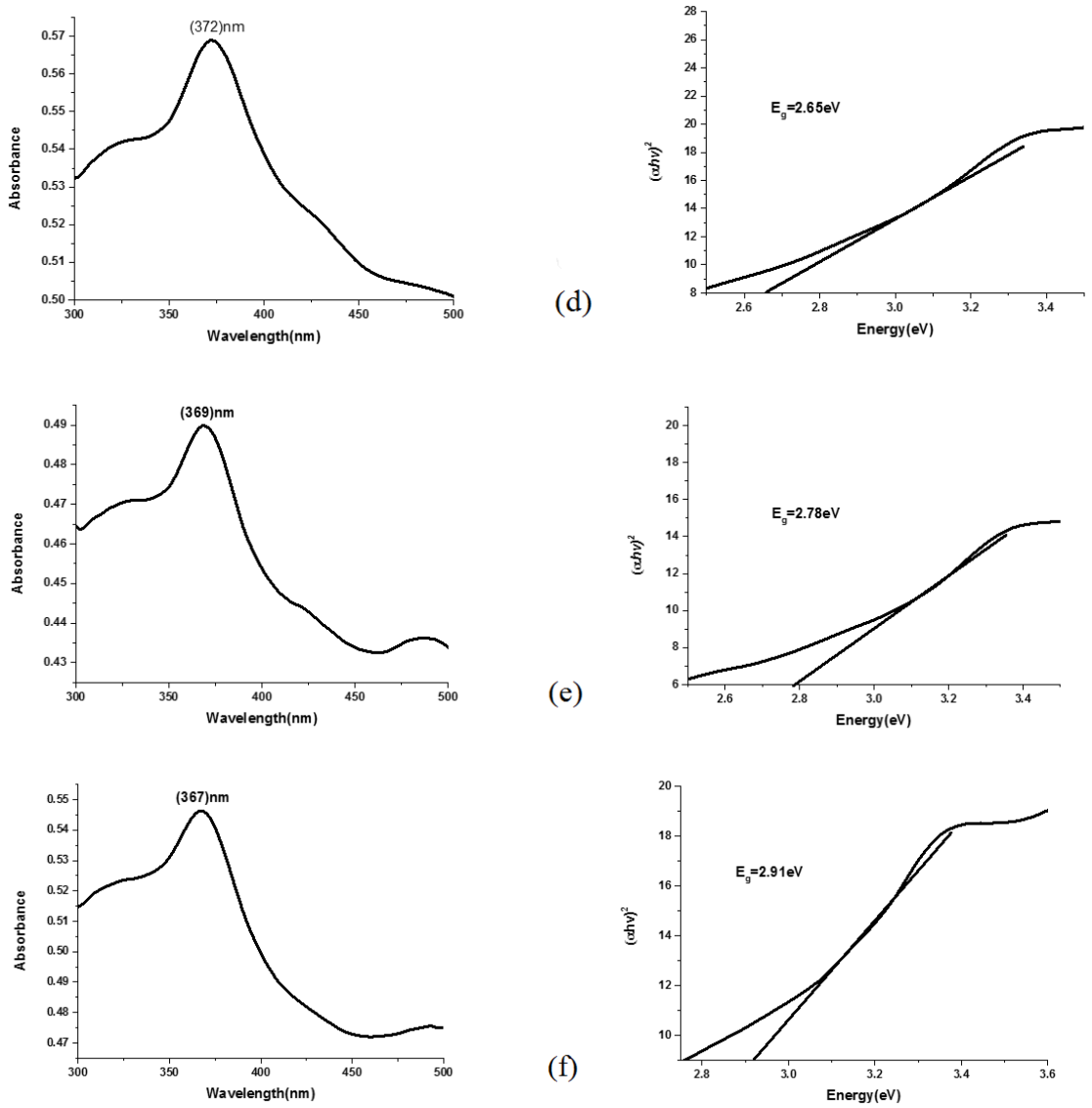


**Figure 16.** UV-Vis. Spectra and Tauc's plots for the energy band gap of the (a) ZnO (b) γ-$Al_2O_3$ (c) GO (d) composite Aerogel of 10% (e) composite Aerogel of 30% (f) composite Aerogel of 50%.

% as anode and different dyes (nano curcumin, methylene blue, and mixed of dyes) as sensitizers.

The changes in $I_{SC}$ and $V_{OC}$ values are caused by a change in the type of dye, which plays an essential role in absorbing photons and stimulating electrons, leading to the generation of electric current [25]. This was observed when using methyl blue or adding it to nano curcumin. The presence of GO and ZnO in the nanocomposite aerogel can be increased the electrical conductivity of photoanode due to act as an electron acceptor and makes it easier for photogenerated electrons to move quickly, it lowers the e-h recombination rates.

**Table 1.** Band gap energies of prepared Nanomaterials.

| Nnaomaterial | Band gap energy(eV) |
|---|---|
| ZnO | 2.6 |
| γ-$Al_2O_3$ | 4.94 |
| GO | 3.2 |
| GO/ZnO/$Al_2O_3$ (10%) | 2.65 |
| GO/ZnO/$Al_2O_3$ (30%) | 2.78 |
| GO/ZnO/$Al_2O_3$ (50%) | 2.91 |

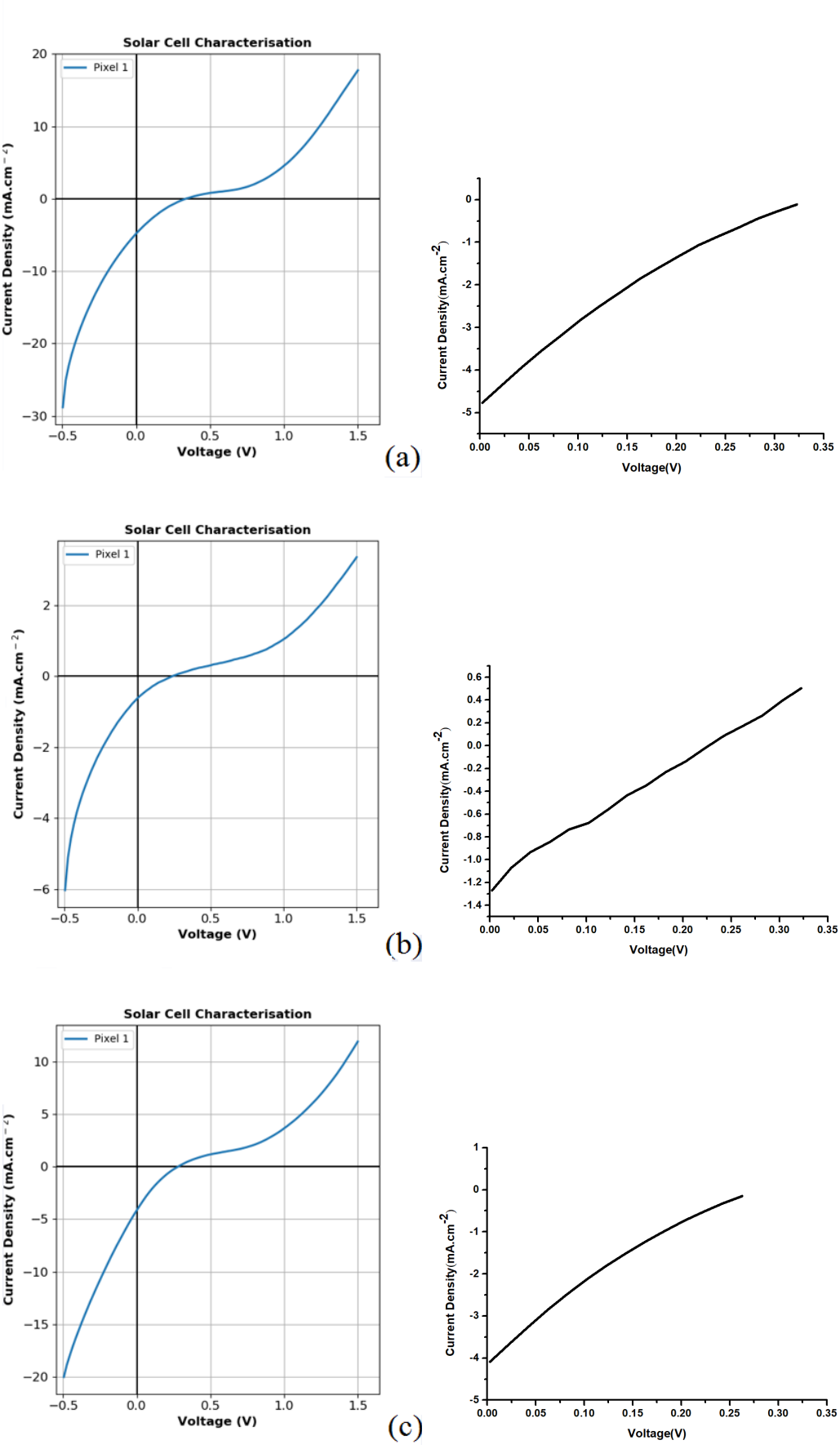


**Figure 17.** I-V Curve of Dye-sensitized solar cell using composite Aerogel 10% as anode and (a) nanocurcumin (b) methylene blue (c) mixed of dyes.

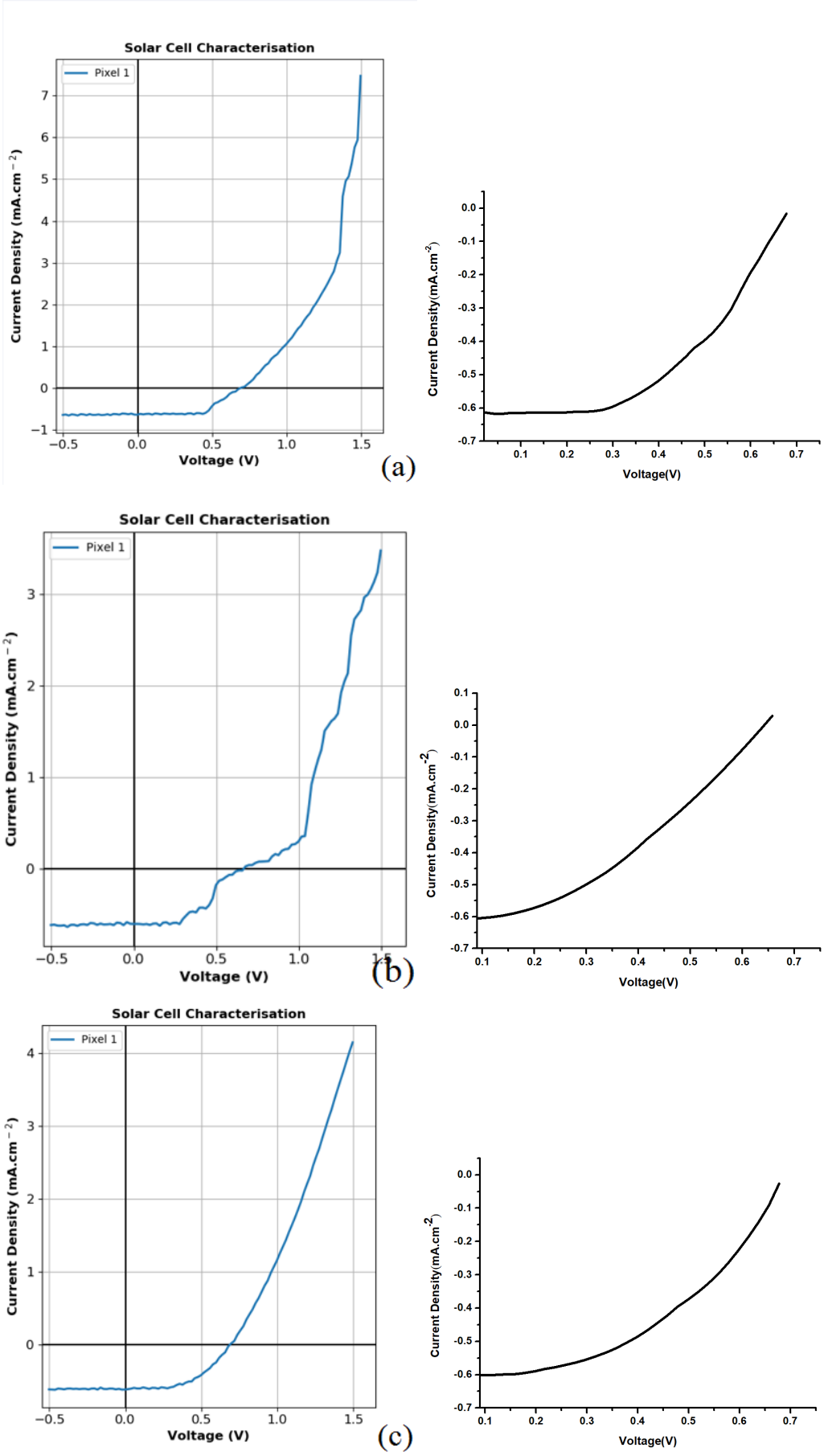


**Figure 18.** I-V Curve of Dye-sensitized solar cell using composite Aerogel 30% as anode and (a) nanocurcumin (b) methylene blue (c) mixed of dyes.

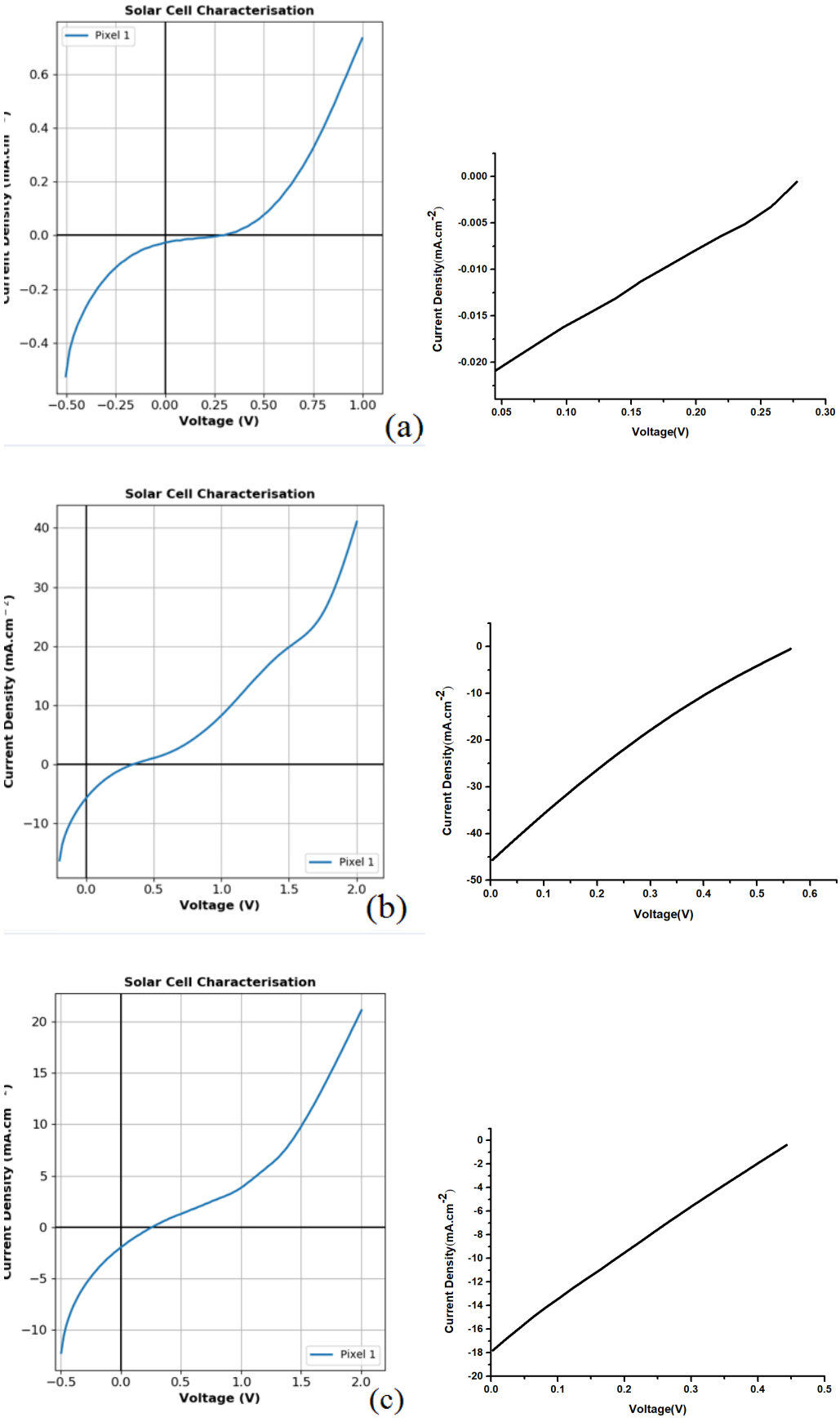


**Figure 19.** I-V Curve of Dye-sensitized solar cell using composite Aerogel 50% as anode and (a) nano curcumin (b) methylene blue (c) mixed of dyes.

**Table 2.** Parameters of dye-sensitized solar cells.

| 10% | | | | |
|---|---|---|---|---|
| Dye | $V_{OC}$ (V) | $I_{SC}$ (mA) | FF | $\eta$% |
| nanocurcumin | 0.338 | 4.9 | 0.187 | 0.31 |
| Methylene blue | 0.228 | 1.27 | 0.24 | 0.07 |
| Mixed of dyes | 0.281 | 4.21 | 0.188 | 0.22 |
| 30% | | | | |
| Dye | $V_{OC}$ (V) | $I_{SC}$ (mA) | FF | $\eta$% |
| nanocurcumin | 0.689 | 0.62 | 0.63 | 0.27 |
| Methylene blue | 0.659 | 0.6 | 0.478 | 0.19 |
| Mixed of dyes | 0.694 | 0.61 | 0.525 | 0.22 |
| 50% | | | | |
| Dye | $V_{OC}$ (V) | $I_{SC}$ (mA) | FF | $\eta$% |
| nanocurcumin | 0.287 | 0.03 | 0.225 | 0.002 |
| Methylene blue | 0.344 | 5.81 | 0.178 | 0.36 |
| Mixed of dyes | 0.259 | 1.98 | 0.225 | 0.12 |

## 4. Conclusion

The successful synthesis and characterization of the GO/ZnO/$Al_2O_3$ nanocomposite aerogel highlight its potential as an excellent photoanode in dye-sensitized solar cells using either nano curcumin or methylene blue as a sensitizer. The results show that when mixed with methylene blue, nano curcumin performs better than used alone. The DSSC fabricated with an optimized photoanode with the above nanocomposite aerogel in different ratios of graphene oxide exhibits the best performance with an $I_{SC}$ of 5.81 mA/cm$^2$, $V_{OC}$ of 0.344 V, FF of 17.8%, with a PCE of 0.36% at a ratio of 50% graphene oxide using methylene blue as sensitizer.

**Authors contributions**
Authors have contributed equally in preparing and writing the manuscript.

**Availability of data and materials**
The data that support the findings of this study are available from the corresponding author, upon reasonable request.

**Conflict of interests**
The authors assert that they do not have any identifiable conflicting financial interests or personal relationships that might be perceived to influence the work presented in this paper.

## References


[1] W. Dequan, L. Xiang, L. Shenghua, L. Leipeng, W. Lei, L. Zexiong, and H. Yonggang. "Fabrication, Structure, Performance, and Application of Graphene-Based Composite Aerogel.". *Mat.*, 15:299, 2022.
DOI: https://doi.org/10.3390%2Fma15010299.

[2] A. Awatef, R. Muhyaddin, K. Yacine, F. A. S. Hatem, S. Mohsen, and C. Goshtasp. "Simulation of melting and solidification of graphene nanoparticles-PCM inside a dual tube heat exchanger with extended surface.". *J. E. Stor.*, 44:103265, 2021.
DOI: https://doi.org/10.1016/j.est.2021.103265.

[3] R. Tharmakularasa, H. G. Fatemeh, V. Dhayalan, R. Punniamoorthy, and S. Meena. "Enhanced Photovoltaic Properties of Dye-Sensitized Solar Cells through Ammonium Hydroxide-Modified (Nitrogen-Doped) Titania Photoanodes.". *I. J. E. Res.*, 12, 2023.
DOI: https://doi.org/10.1155/2023/1090174.

[4] H. H. Nguyen. "Graphene-Based Material for Fabrication of Electrodes in Dye-Sensitized Solar Cells.". pages 1–19, 2019.
DOI: https://doi.org/10.5772/intechopen.93637.

[5] M. Larisa and C. Cristiana. "Aerogel, a high-performance material for thermal insulation - A brief overview of the building applications.". *E3S Web of Conf.*, page 111, 2019. URL 10.1051/e3sconf/2019111060.

[6] J. Luke, J. D. Lina, S. Omnia, M. Muqoyyanah, A. B. Suriani, D. B. Muhammad, and M. Amine El. "Hybrid Organic–Inorganic Perovskite Halide Materials for Photovoltaics towards Their Commercialization.". *Polym.*, 14:1–27, 2022.
DOI: https://doi.org/10.3390/polym14051059.

[7] A. Atli, A. Atilgan, and A. Yildiz. "Multi-layered $TiO_2$ photoanodes from different precursors of nanocrystals for dye-sensitized solar cells.". *Sol. E.*, 173:752–758, 2018.
DOI: https://doi.org/10.1016/j.solener.2018.08.027.

[8] N. T. Sethu and S. Shanmugan. "Towards sustainable solar cells: Unveiling the latest developments in bio-nano materials for enhanced DSSC efficiency.". *Clean Eny.*, 8:238–257, 2024.
DOI: https://doi.org/10.1093/ce/zkae031.

[9] N. Samantha, M. Edigar, A. O. Moses, and O. N. Vincent. "Tuning the Properties of Reduced Graphene Oxide $Sr_{0.7}Sm_{0.3}Fe_{0.4}Co_{0.6}O_3$ Nanocomposites as Potential Photoanodes for Dye Sensitized Solar Cells.". *J. Ele. Mat.*, 52:5843–5860, 2023.
DOI: https://doi.org/10.1007/s11664-023-10526-3.

[10] N.G. Aminah, A. L. d. S. Otávio, H. Layla, P. B. Bianca, B. Mohamed, and B. Stefano. "Graphene Oxide (GO) Materials-Applications and Toxicity on Living Organisms and Environment. ". *J. Func. Biomat.*, 13:1–28, 2022.
DOI: https://doi.org/10.3390/jfb13020077.

[11] M. Savisha, W. L. Foo, O. Azimah, M. Abreeza, A. R. Nasrudin, H. T. Chun, A. Huda, H. V. Chun, R. Mamat, W. Edy, and S. O. Cheen. "Zinc oxide/graphene nanocomposite as efficient photoelectrode in dye-sensitized solar cells: Recent advances and future outlook.". I. J. E. R.:1–19, 2022.
DOI: https://doi.org/10.1002/er.7722.

[12] L. M. P. Sai, D. K. Alka, and C. Ushasri. "Various Extraction Techniques of Curcumin-A Comprehensive Review.". *ACSO mega*, 8:34868–34878, 2023.
DOI: https://doi.org/10.1021%2Facsomega.3c04205.

[13] S. K. Ayoub, O. A. Fuad, and Z. M. Najat. "Green Synthesis and Evaluation of ZnO NPs and study the effect of Their toxic on Honey Bee (Apis mellifera) Bag. S. J. ". *Proc Inst Mech Eng C: J Mech Eng Sci.*, 21:2124–2136, 2024.
DOI: https://doi.org/10.21123/bsj.2023.8664.

[14] H. Yonggang, L. Shenghua, L. Leipeng, and L. Xiang. "High-quality preparation of graphene oxide via the Hummers' method: Understanding the roles of the intercalator, oxidant, and graphite particle size.". *Cer. I.*, 46:2392–2402, 2020.
DOI: https://doi.org/10.1016/j.ceramint.2019.09.231.

[15] G. Santamaría-Juárez, E. Gómez-Barojas, E. Quiroga-González, E. Sánchez-Mora, and J. D. Santamaría-Juárez. "Preparation and Characterization of Reduced Graphene Oxide/Titanium Dioxide Composites by Hydrothermal Method.". *Eur. J. Eng. Res. and Sci.*, 4:165–173, 2019.
DOI: https://doi.org/10.24018/ejers.2019.4.9.1364.

[16] N. M. Sabah, H. A. Alyaa, A. K. Quraish, and F. M. Neean. "Synthesis of Nano curcumin Via Sol-Gel/Ultrasonic Processors Route and Improving their properties by Microwaves-Induced Plasma.". *J. Phy.*, 1660:012042, 2020.
DOI: https://doi.org/10.1088/1742-6596/1660/1/012042.

[17] W. Tian-Chiuan, H. Wei-Ming, T. Jenn-Kai, C. Cheng-En, and M. Teen-Hang. "Effect of Photoanode Process Sequence on Efficiency of Dye-Sensitized Solar Cells.". *Coat.*, 14:1–11, 2024.
DOI: https://doi.org/10.3390/coatings14030304.

[18] G. Giphin, S. Y. Raja, and M. E. Anu. "Fabrication of Dye-Sensitized Solar Cells using natural flower dye extracts: A study on performance analysis and solar dye degradation. ". *Eny. Sour. Part A*, pages 1–15, 2020.
DOI: https://doi.org/10.1080/15567036.2020.1796849.

[19] E. Selva Esakki, R. Sarathi, S. S. Meenakshi, and D. L. Renuga. "Fabrication of Dye Sensitized Solar Cells using Ixora Macrothyrsa.". *Mat. Today: Proceedings.*, 47:2182–2187, 2020.
DOI: https://doi.org/10.1016/j.matpr.2021.05.672.

[20] R. A. Kazi, Md. Ashaduzzaman, C. P. Shujit, R. N. Mithun, B. Snahasish, S. Otun, R. Md. Mizanur, B. Shukanta, and D. A. Tutu. "Microwave assisted synthesis of zinc oxide (ZnO) nanoparticles in a noble approach: Utilization for antibacterial and photocatalytic activity.". *SN App. Sci.*, 2:955, 2020.
DOI: https://doi.org/10.1007/s42452-020-2762-8.

[21] K. K. V. Ashok, B. Lakshminarayana, D. Suryakalab, and Ch. Subrahmanyam. "Reduced graphene oxide supported ZnO quantum dots for visible light-induced simultaneous removal of tetracycline and hexavalent chromium.". *RSC Adv.*, 10:20494, 2020.
DOI: https://doi.org/10.1039/d0ra02062a rsc.li/rsc-advances.

[22] I. Boukhoubza, M. Khenfouch, M. Achehboune, B. M. Mothudi, I. Zorkani, and A. Jorio. "X-ray diffraction investigations of nanostructured ZnO coated with reduced graphene oxide. ". *J. Phy.*, 10: 1292, 2019.
DOI: https://doi.org/10.1088/1742-6596/1292/1/012011.

[23] B. Haotian, L. Jingjing, Y. Jiahao, C. Zhongghao, W. Wenjie, Z. Shiyu, and Z. Peixi. "Synthesis and characterization of zinc oxide-graphene oxide nanocomposites for electrocatalytic detection of rutin.". *Alex. Eng. J.*, 91:486–493, 2024.
DOI: https://doi.org/10.1016/j.aej.2024.02.018.

[24] B. Issam, K. Mohammed, A. Mohamed, L. Liviu, C. G. Aurelian, E. Monika, C. Aurelian, G. Mohammed, M. M. Bakang, J. Anouar, and Z. Izeddine. "Graphene Oxide Concentration Effect on the Optoelectronic Properties of ZnO/GO Nanocomposites.". *Nanomat.*, 10:1532, 2020.
DOI: https://doi.org/10.3390/nano10081532.

[25] D. Van-Duong. "Comment on "Energy storage via polyvinylidene fluoride dielectric on the counter electrode of dye-sensitized solar cells".". *J. P. Sour.*, 337:125–129, 2016.
DOI: https://doi.org/10.1016/j.jpowsour.2013.09.094.